

Generating fractal rough surfaces with the spectral representation method

Yuechang Wang , Abdullah Azam, Mark CT Wilson, Anne Neville and Ardian Morina 

Proc IMechE Part J:
J Engineering Tribology
2021, Vol. 235(12) 2640–2653
© IMechE 2021



Article reuse guidelines:
sagepub.com/journals-permissions
DOI: 10.1177/13506501211049624
journals.sagepub.com/home/pij



Abstract

The application of the spectral representation method in generating Gaussian and non-Gaussian fractal rough surfaces is studied in this work. The characteristics of fractal rough surfaces simulated by the spectral representation method and the conventional Fast Fourier transform filtering method are compared. Furthermore, the fractal rough surfaces simulated by these two methods are compared in the simulation of contact and lubrication problems. Next, the influence of low and high cutoff frequencies on the normality of the simulated Gaussian fractal rough surfaces is investigated with roll-off power spectral density and single power-law power spectral density. Finally, a simple approximation method to generate non-Gaussian fractal rough surfaces is proposed by combining the spectral representation method and the Johnson translator system. Based on the simulation results, the current work gives recommendations on using the spectral representation method and the Fast Fourier transform filtering method to generate fractal surfaces and suggestions on selecting the low cutoff frequency of the power-law power spectral density. Furthermore, the results show that the proposed approximation method can be a choice to generate non-Gaussian fractal surfaces when the accuracy requirements are not high. The MATLAB codes for generating Gaussian and non-Gaussian fractal rough surfaces are provided.

Keywords

Fractal rough surface generation, cutoff frequency, non-Gaussian, spectral representation method

Date received: 20 May 2021; accepted: 12 September 2021

Introduction

Many rough surfaces are nearly self-affine fractal within a wide range of scales, such as road surfaces, surfaces produced by fracture, and sandblasted surfaces.¹ A self-affine fractal surface looks the same when part of the surface is magnified. Moreover, the roughness parameters of self-affine fractal surfaces, such as the root-mean-square roughness and average surface curvature, are related to the measurement length scale.^{2–5} Most of the widely used roughness parameters are determined based on a discrete surface height data set with a specific measurement length scale,^{6,7} making it impossible to use these parameters to characterize the self-affine fractal surfaces across scales. Therefore, a scale-invariant parameter, the fractal dimension D , becomes the key to characterize roughness across scales. For a self-affine fractal surface, the fractal dimension D can be obtained through its power spectral density (PSD), which follows a power-law relationship shown in the following.

$$S(q) \sim q^{-2(H+1)} \quad (1)$$

where $S(q)$ represents the PSD, q is the angular frequency, and H is the Hurst exponent, related to D through $H=3-D$.⁸

In realistic surfaces, the value of q is between the low and high cutoff frequencies.

As the power-law PSD characterizes a self-affine fractal surface across scales, it has been widely used to model interfacial phenomena considering multiscale roughness, for example, contact, friction, and adhesion. These phenomena play an essential role in engineering systems, such as micro-electro-mechanical systems (MEMS), biomechanics, bearings, gears, and sealings. In these systems, the dry contact (without lubricant) between rough surfaces is one of the key factors in analyzing their performance. Many efforts have been put into the study of contact between self-affine fractal surfaces.^{9–13} In addition to the dry contacts, some researchers studied lubricated contacts with fractal surfaces, for example, Li and Yang¹⁴ studied the influence of fractal surfaces on

Institute of Functional Surfaces, School of Mechanical Engineering, University of Leeds, UK

Corresponding author:

Yuechang Wang, Institute of Functional Surfaces, School of Mechanical Engineering, University of Leeds, Leeds LS2 9JT, UK.
Email: y.wang1@leeds.ac.uk

elastohydrodynamic lubrication (EHL) and Zhang et al.¹⁵ studied a thrust bearing in a mixed lubrication regime with fractal surfaces.

Most of the models mentioned above require fractal surfaces realized at specific frequency ranges. Compared with surface measurement, numerical simulation has been a popular way to obtain rough surfaces due to its convenience and economy. A large number of papers have been published about the simulation of rough surfaces.¹⁶ It should be noted that simulated rough surfaces only represent surface features within one specific evaluation area. If the evaluation area changes, the parameters used to simulate rough surfaces should be changed accordingly. At the very beginning, the mainstream in rough surface simulation is to generate surfaces with exponential PSD, which is non-fractal. There are two widely accepted conventional methods: the moving average (MA) time series model and the spectral representation method (SRM). The MA model can be implemented by different algorithms.^{17–20} One of them, widely used, is the two-dimensional (2-D) digital filter method developed by Hu and Tonder,¹⁸ generating surfaces with Gaussian or non-Gaussian height distributions. The SRM was first used by Newland²¹ and Wu²² to simulate Gaussian rough surfaces. The difficulties of using the SRM to simulate non-Gaussian surfaces were studied by Wu,²³ then Wang et al.²⁴ Through these efforts, the SRM can be used in simulating non-Gaussian surfaces. Wu²² and Wang et al.²⁴ pointed that SRM has better performance in generating rough surfaces than the 2-D digital filter method. When generating non-Gaussian surfaces, the Johnson translator system is usually used in the 2-D digital filter method or the SRM. The Johnson translator system provides a group of transformation curves, which translate Gaussian random series to non-Gaussian series, and vice versa.²⁵

In terms of generating fractal surfaces, they were first studied in simulating fractal images by Voss^{26,27} and Saube²⁸ in the 1980s. They proposed several methods, including the fast Fourier transform (FFT) filtering method, random midpoint displacement (RMD), successive random additions, and Weierstrass–Mandelbrot (W–M) random fractal function. Others inherited these methods to simulate fractal rough surfaces. Majumdar and Tien⁴ first utilized the W–M fractal function method, whose PSD approximately follows the power law, to characterize and simulate the fractal roughness. Li and Yang¹⁴ also used the W–M fractal function method. Ganti and Bhushan⁵ first utilized the FFT filtering method to simulate fractal surfaces. Wu²⁹ compared the W–M fractal function method, FFT filtering method, and successive random addition method in generating fractal surfaces. It turned out that the FFT filtering method reproduces the power-law PSD better than the other two methods. Müser et al.,⁹ Borri and Paggi,³⁰ and Zhang et al.¹⁵ used the FFT filtering method as well. Besides the FFT filtering method and the W–M function, the RMD is another common choice in studies, for example, Pei et al.,³¹ Bonari et al.,³² and

Vakis et al.³³ simulated fractal surfaces by the RMD for contact analysis. In addition to the methods above, Papangelo et al.¹³ and Putignano et al.³⁴ developed a spectral method, which is similar to the FFT filtering method, for simulating fractal surfaces.

The methods above are the current mainstream approaches for generating fractal surfaces. One point worthy of attention is that all these methods generate fractal surfaces with Gaussian height distribution. Only a few researchers^{35,36} studied the generation of fractal surfaces with non-Gaussian height distribution. Another surprising observation is the lack of mutual learning between the simulation of fractal and non-fractal surfaces, considering the only difference between them is the expression of PSD. It seems that the development of fractal and non-fractal surface simulations are primarily independent of each other. One exception found in the literature is that Yastrebov et al.¹² used the 2-D digital filter method¹⁸ to simulate the Gaussian fractal surfaces. Furthermore, Yastrebov et al.¹² and several researchers^{37,38} reported the influence of the PSD cutoff frequencies on the simulated fractal surfaces and corresponding contact simulations. However, such phenomena are ignored by most mainstream methods of simulating fractal surfaces.

Based on the literature above, although the methods for generating fractal surfaces have succeeded in many applications, they still have two shortcomings that cannot be ignored. The first is the lack of methods for non-Gaussian fractal surfaces simulation, and the other is the lack of attention in choosing the cutoff frequencies of the power-law PSD. This paper seeks to make some progress in overcoming these two shortcomings.

Inspired by the well-proven methods for simulating non-Gaussian surfaces with exponential PSD, a possible solution for simulating non-Gaussian fractal surfaces is using power-law PSD instead of the exponential PSD in those methods. Bearing this idea in mind, we noticed the high similarity between the SRM and the FFT filtering method. They have almost the same theoretical fundamentals and equations (detailed comparisons are shown in section FFT filtering method and SRM). Moreover, both have been proven to be efficient and accurate in the literature. Therefore, to generate non-Gaussian fractal surfaces, we first compare the performance of the SRM and the FFT filtering method in detail, then study the simulation of non-Gaussian fractal surfaces. In the meantime, the influence of cutoff frequencies of the power-law PSD on the simulated fractal surfaces is studied.

In summary, the current study is organized as follows. The FFT filtering method and the SRM are first compared theoretically. Then, the influences of using these two methods on the characteristics of simulated fractal rough surfaces are compared. Furthermore, the simulated surfaces are used to predict the performance of contact of rough surfaces and EHL. The differences resulting from these two simulation methods are highlighted. Next, the influence of low and high cutoff frequencies of the PSD on the simulated fractal surfaces is clarified. Finally,

simulating non-Gaussian fractal surfaces are studied, and a simple approximation method is proposed.

FFT filtering method and SRM

Theoretically, the FFT filtering method^{5,26–30} and the SRM^{21,22,39} have the same aim: generating random series with the desired PSD. They construct complex Fourier coefficients, where the amplitude terms follow the desired PSD. For the phase terms, they use random phase values following the same distribution when simulating Gaussian surfaces. Then, a sample of the random surfaces is obtained by applying the inverse Fourier transform to the Fourier coefficients constructed. Therefore, the equations of the FFT filtering method and the SRM have the same form, which is shown as equation (2):

$$z_{ij} = \sum_{k=0}^{M-1} \sum_{l=0}^{N-1} B_{kl} \exp(i\phi_{kl}) \exp\left[i\left(\frac{2\pi ki}{M} + \frac{2\pi lj}{N}\right)\right] \quad (2)$$

where,

$$i = 0, 1, 2, \dots, M - 1$$

$$j = 0, 1, 2, \dots, N - 1$$

In equation (2), the generated surface has a mesh of $M \times N$, z_{ij} is the surface height at the point (i, j) , B_{kl} is the amplitude related to the PSD value at the point (k, l) , and ϕ_{kl} represents the random phase at the point (k, l) . All ϕ_{kl} values are distributed uniformly over the interval $[0, 2\pi]$ when simulating surfaces with the Gaussian height distribution. Equation (2) can be efficiently calculated by the FFT algorithm. One thing to note is that some restrictions in calculating B_{kl} and ϕ_{kl} are a prerequisite for using the FFT algorithm (see Appendix A).

The differences between the FFT filtering and SRM result from the calculation of the coefficient B_{kl} . In the SRM, B_{kl} is calculated as follows,^{21,22,39}

$$B_{kl} = (S_{kl})^{1/2} \quad (3)$$

where S_{kl} represents the PSD values. However, in the FFT filtering method, the equation for B_{kl} is^{5,26–30}

$$B_{kl} = \alpha_{kl}(S_{kl})^{1/2} \quad (4)$$

where α_{kl} is a random number following uniform distribution over the interval $[0, 1]$.

Based on the expressions of equations (3) and (4), it can be inferred that equation (4) results in the generated surfaces having the target PSD in average, but equation (3) can generate surfaces whose PSD is identical to the required one without considering the numerical calculation errors. In other words, the use of equation (4) makes the FFT filtering method introduce one more source of uncertainties in the simulated surfaces compared with the SRM. It should be noted that both methods have a common source of uncertainties, which is the random phase ϕ_{kl} .

The power-law PSD used to generate fractal rough surfaces is referred to by Müser et al.,⁹ which is

$$S(q) = S(q_r) \times \begin{cases} 1 & \text{for } \lambda_r < 2\pi / q \leq L \\ (q / q_r)^{-2(1+H)} & \text{for } \lambda_s \leq 2\pi / q \leq \lambda_r \\ 0 & \text{else.} \end{cases} \quad (5)$$

Here, q is the magnitude of the angular frequency vector $q = (q_x, q_y)$, and L is the linear dimension in the x and y directions, equalling 0.1 mm. $q_r = 2\pi/\lambda_r$ is the roll-off angular frequency, $\lambda_r = 20 \mu\text{m}$ is the corresponding roll-off wavelength, and $\lambda_s = 0.1 \mu\text{m}$ sets the short-wavelength cutoff. H is the Hurst roughness exponent, which equals 0.8. $S(q_r)$ denotes the PSD amplitude and is related to the variance (σ^2) of the simulated surfaces. The root-mean-square roughness (standard deviation (SD) σ) of the simulated surfaces is 0.762 μm .

Simulation of non-Gaussian rough surfaces

Many conventional and widely used methods of simulating non-Gaussian rough surfaces^{18–20,24,40} are based on the Johnson translator system.²⁵ The Johnson translator system includes three types of transformation curves, which are as follows.

$$S_U: x = v + \delta \sinh^{-1}\left(\frac{\eta - \xi}{\lambda}\right) \quad (6)$$

$$S_B: x = v + \delta \ln\left(\frac{\eta - \xi}{\xi + \lambda - \eta}\right) \quad (7)$$

$$S_L: x = v + \delta \ln\left(\frac{\eta - \xi}{\lambda}\right) \quad (8)$$

where x denotes the Gaussian series, η is the non-Gaussian series, and $\nu, \delta, \xi, \lambda$ are the parameters derived by Hill's algorithm⁴¹ by the first four moments of η . The first four moments of a random series are mean (μ), variance (σ^2), skewness (Ssk), and kurtosis (Sku). Francisco and Brunetiere⁴² pointed out that the conventional Johnson translator system cannot generate highly accurate random series with specific skewness and kurtosis values. They provided a rather complicated hybrid method for simulating non-Gaussian surfaces. Nevertheless, the Johnson translator system is used in this study as it is easy to use and widely accepted.

While transferring the Gaussian series to the non-Gaussian series, the PSD will be distorted. Such distortion of PSD needs to be corrected before it is used to simulate non-Gaussian surfaces. To tackle this problem, Wang et al.²⁴ used an iteration method to approximate the desired PSD, which is compatible with the translation from the Gaussian to the non-Gaussian series. The method of Wang et al.²⁴ first fits the Johnson translator system by the target Ssk and Sku values and provides a

translation process that translates the Gaussian series to the target non-Gaussian series. Based on the relationship between the autocorrelation function (ACFs) before and after the translation, an underlying PSD compatible with the non-Gaussian height distribution is iteratively approximated. Next, with this underlying PSD, a Gaussian rough surface can be simulated by the SRM. Finally, the simulated Gaussian surface is translated to the required non-Gaussian surface by the fitted Johnson curve. This non-Gaussian surface should have both the required PSD and target Ssk and Sku with high accuracy. The detailed procedures of this method can be found in the work of Wang et al.²⁴ In the current study, this method is tested with the power-law PSD.

Results and discussion

Surfaces generated by the FFT filtering method and SRM

Gaussian fractal rough surfaces with a grid size of 2048×2048 were generated by the FFT filtering method and SRM. As the FFT filtering method has two sources of uncertainties (amplitude and phase terms in equation (2)), while the SRM has one (phase term in equation (2)), the generation of random samples of these two methods is different in the current study.

For the FFT filtering method, the random samples were selected by following rules to highlight the influence of uncertainties caused by the amplitude term. For each set of fixed phase term ϕ_{kl} values, 1000 fractal surfaces were generated with altering B_{kl} values by equation (4). Furthermore, to show the influence of the two uncertainty sources preliminarily, 100 different sets of phase term values were used. For the SRM, as the phase term is the only uncertainty source in equation (2), 1000 fractal surfaces were simulated with altering ϕ_{kl} values, while the B_{kl} values were the same as calculated by equation (3).

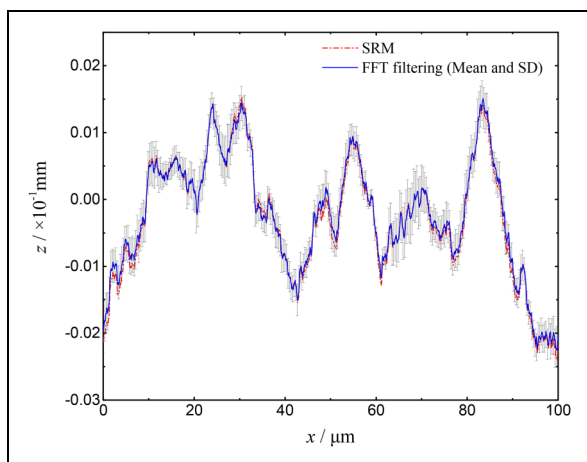


Figure 1. Central line profiles of fractal surfaces simulated by the FFT filtering method and SRM. FFT: fast Fourier transform; SRM: spectral representation method.

Figure 1 shows the central line profiles, which is the 1024th row of the simulated surfaces. The surfaces used to plot this figure were simulated with the same ϕ_{kl} values. Therefore, the central line profile of the surface simulated by the SRM is a single line, while the FFT filtering method provides 1000 central line profiles. The mean profile of these 1000 profiles was plotted, and their SD was also plotted to show the uncertainties. Figure 1 clearly shows that the mean central line profile of surfaces simulated by the FFT filtering method agrees well with the single profile generated by the SRM. The SD corresponding to the profiles resulted from the FFT filtering method has a magnitude of $0.3 \mu\text{m}$.

Figure 2 shows the target PSD, mean PSD of the surfaces simulated by the SRM, and the mean PSD of the surfaces simulated by the FFT filtering method. Again, the SD values were taken to illustrate the uncertainties. It clearly shows that the mean PSD of the surfaces simulated by the SRM perfectly matches the target one. Furthermore, the most significant SD value is at the magnitude of 1×10^{-19} , which is still too small to plot in Figure 2. Such a result means that every single surface generated by the SRM can reproduce the target PSD very well. In comparison, the mean PSD resulted from the FFT filtering method approximately follows the target one and has significant deviations occurring at some frequencies.

To further characterize the simulated surfaces, several widely used roughness parameters were calculated, including the skewness (Ssk), kurtosis (Sku), root-mean-square gradient (Sdq), summit density (Sds), and mean summit radius (Rc). Ssk and Sku can help to characterize the surface height distribution. Sdq , Sds , and Rc are based on the definition of the summit of roughness. Detailed information on the calculation of these parameters is given in Appendix B. One more thing worthy of knowing about these parameters is that they are traditional statistical roughness parameters and cannot comprehensively characterize rough surfaces. Some parameters

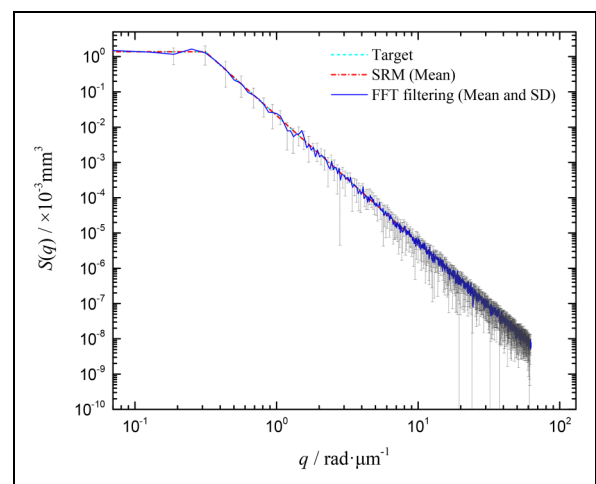


Figure 2. PSD of fractal surfaces simulated by the FFT filtering method and SRM. FFT: fast Fourier transform; SRM: spectral representation method; PSD: power spectral density.

defined by morphological methods can enhance the analysis of simulated surfaces in future work.⁴³

Figure 3 shows the roughness parameters calculated based on the surfaces simulated by the FFT filtering method. The abscissa represents the 100 different groups of ϕ_{kl} values. For each group of ϕ_{kl} , the roughness parameters of the 1000 simulated surfaces with randomized B_{kl} values were averaged, and the corresponding SDs were plotted to show the uncertainties. It can be seen that uncertainties in the ϕ_{kl} and B_{kl} values affect the output roughness parameters. In particular, Ssk , Sku , and Sds are significantly influenced by ϕ_{kl} , while the Sdq and Rc are not sensitive to it. The reason should be that the phase term ϕ_{kl} determines the height distribution of the simulated surfaces theoretically. The Ssk and Sku are the parameters to characterize the height distribution, and the Sds is closely related to the height distribution. Thus, these three parameters are sensitive to the change of ϕ_{kl} . As for the Sdq and Rc , they are more relevant to the spatial information of the roughness, which is mainly dominated by the PSD in theory. Hence, they are not influenced much by changing the ϕ_{kl} values.

Unlike the uncertainties introduced by the ϕ_{kl} , the uncertainties in the B_{kl} have significant influences on all the five roughness parameters. The magnitude of such influences on each parameter can be estimated by taking the average, and SD of the standard deviation (SD) values caused by the uncertainties in the B_{kl} with the 100 different groups of ϕ_{kl} values. The corresponding results are listed in Table 1. The mean value of the SD values is different for different roughness parameters, while the SD of the SD values is tiny for all the five roughness parameters. This result means that the uncertainties of a specific roughness parameter caused by the uncertain B_{kl} are at the same magnitude with different ϕ_{kl} values. Moreover, the two sources of uncertainties (amplitude and phase) in the FFT filtering method are probably irrelevant regarding the influences on the roughness parameters discussed in this paper.

Figure 4 plots the roughness parameters calculated based on the surfaces simulated by the SRM. The abscissa

represents 1000 different groups of ϕ_{kl} values. Once more, it shows that different sets of ϕ_{kl} values dramatically influence the Ssk , Sku , and Sds values but hardly affect the Sdq and Rc . The mean Ssk , Sku , and Sds values of the 1000 simulated surfaces are 0.004 , 2.98 , and $8.8 \mu\text{m}^{-2}$, with a SD of 0.11 , 0.17 , and 0.025 , respectively. It is expected that the mean Ssk and Sku values with different groups of ϕ_{kl} values approach the values of an ideal Gaussian distribution, which are 0 for the Ssk and 3 for the Sku . When the ϕ_{kl} is fixed (see Figure 3), only considering the uncertainties in the B_{kl} cannot get mean Ssk and Sku values approaching the ideal Gaussian distribution, but some values determined by the phase term used. Therefore, the uncertainties in the ϕ_{kl} (phase term) have a more important role in simulating Gaussian surfaces than the uncertainties in the B_{kl} (amplitude term). The other point worthy of notice is the comparisons between the SDs of Ssk , Sku , and Sds caused by the uncertain ϕ_{kl} and B_{kl} . For the Ssk and Sku , the SDs caused by the uncertain ϕ_{kl} (0.11 and 0.17) are more significant than those caused by the uncertain B_{kl} (0.06 and 0.10 , see Table 1). For the Sds , the uncertain ϕ_{kl} results in a standard deviation of 0.025 , less than the SD caused by the uncertain B_{kl} (0.06 , see Table 1).

In addition to the comparisons of roughness profiles and parameters, a more critical issue is to compare the surfaces simulated by the FFT filtering method and the SRM in tribological applications. Therefore, two classic tribological applications, contact between rough surfaces and EHL, are conducted.

Contact of rough surfaces. The parameters set for contact simulation are extracted from Müser et al.⁹ The fractal rough surfaces are pressed down to a flat rigid surface. The equivalent Young's modulus is $E^* = 25 \text{ MPa}$. The applied load varies from $0.0001E^*$ to $0.9E^*$. To highlight the influence of uncertainties in the B_{kl} and save computational resources, 100 surfaces simulated by the FFT filtering method, and one surface simulated by the SRM with the same ϕ_{kl} values were used in the contact simulation. The numerical procedures for solving these contact problems can be found in the work of Marklund et al.⁴⁴

Three parameters were calculated during the simulations: the relative contact area a_r , mean contact pressure p_c , and mean gap u_g . The relative contact area a_r is the ratio of the real contact area to the nominal contact area. The mean contact pressure p_c is the arithmetic mean of the contact pressure values at each contact node. The

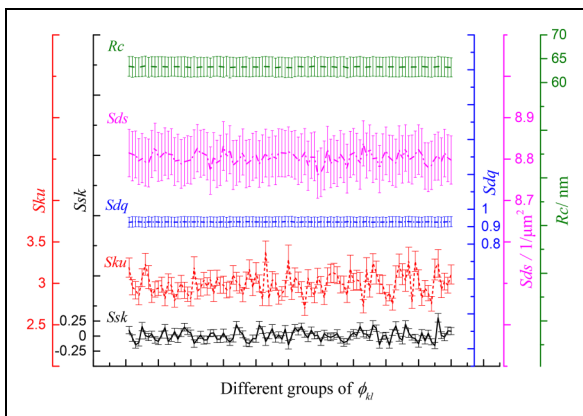


Figure 3. Roughness parameter values of fractal surfaces simulated by fast Fourier transform (FFT) filtering method.

Table 1. Mean and standard deviation of the SD values caused by the uncertainties in the B_{kl} .

Parameter	Mean of SD values	The SD of SD values
Ssk	0.06	0.0063
Sku	0.10	0.0209
Sdq	0.29	0.0071
$Sds/\mu\text{m}^{-2}$	0.06	0.0014
Rc/nm	2.05	0.0490

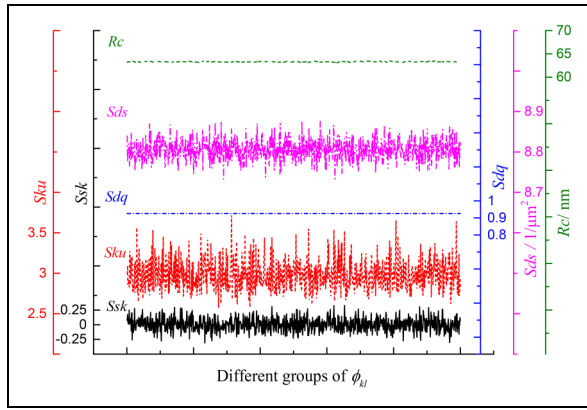


Figure 4. Roughness parameter values of fractal surfaces simulated by the spectral representation method (SRM).

mean gap u_g is the mean height of the deformed rough surface. These parameters were plotted versus applied loads, respectively (Figures 5 to 7).

The results show that, on average, the a_r , p_c and u_g values calculated from the contact of surfaces simulated by the FFT filtering method agree well with those using surfaces simulated by the SRM. Figure 5 shows that the relative contact area a_r values are slightly influenced by using the FFT filtering method with a wide range of applied loads, especially with smaller applied loads. Figure 6 illustrates that with smaller applied loads, the mean contact pressure p_c values are significantly influenced when the surfaces simulated by the FFT filtering method are used. With smaller applied loads, the contact spots and contact pressures are easily affected by small asperities, which results in more significant uncertainties in the a_r and p_c values. As for the mean gap, it can be seen in Figure 7 that the u_g values are sensitive to the use of the FFT filtering method with larger applied loads. This result should be because large applied loads lead to more significant interactions

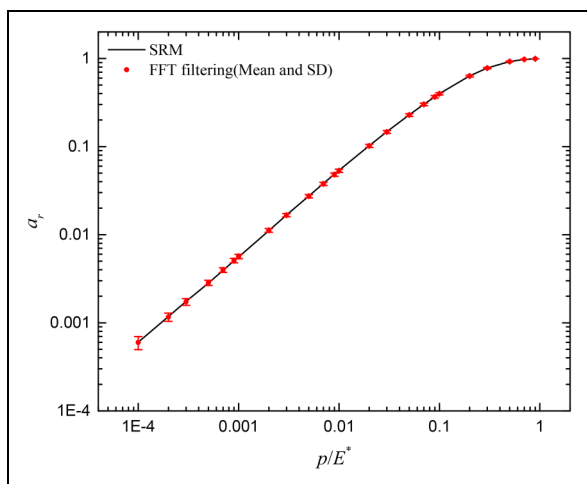


Figure 5. Relative area a_r values with fractal surfaces simulated by FFT filtering and SRM. FFT: fast Fourier transform; SRM: spectral representation method.

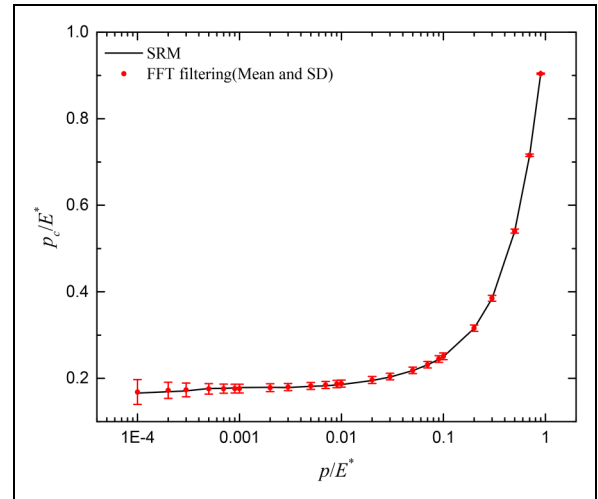


Figure 6. Mean contact pressure p_c values with fractal surfaces simulated by FFT filtering and SRM. FFT: fast Fourier transform; SRM: spectral representation method.

between asperities. Thus, the surface deformation is more sensitive to the changes in asperity distribution, resulting in more significant deviations in the u_g values. Another point worth noting from Figures 5 to 7 is that the choice of method does not affect the dry contact simulation result much. This finding allows a direct comparison between dry contact simulations that used the FFT filtering method and the SRM.

EHL simulation. A typical point contact EHL problem defined in the work of Venner and Lubrecht⁴⁵ is used in the current work. The corresponding parameters are listed in Table 2. The transient Reynolds equation is used. Ten surfaces simulated by the FFT filtering method and one surface simulated by the SRM with the same ϕ_{kl} values are used to reduce the calculation

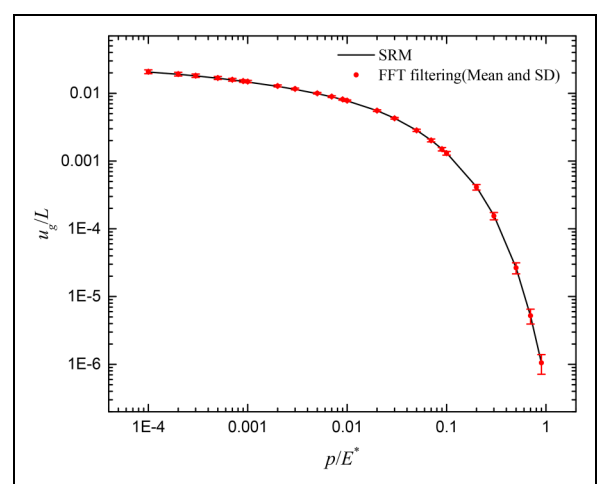
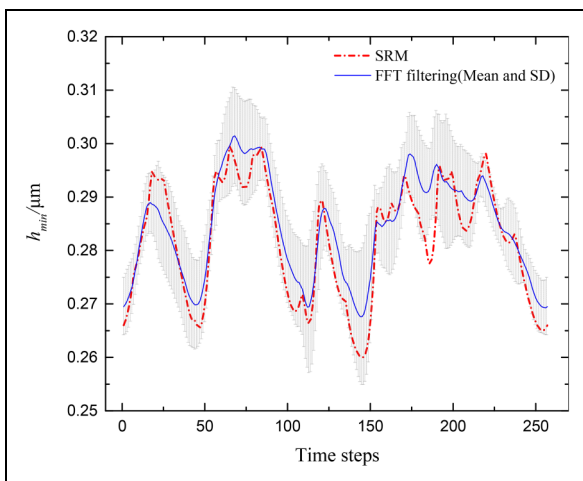
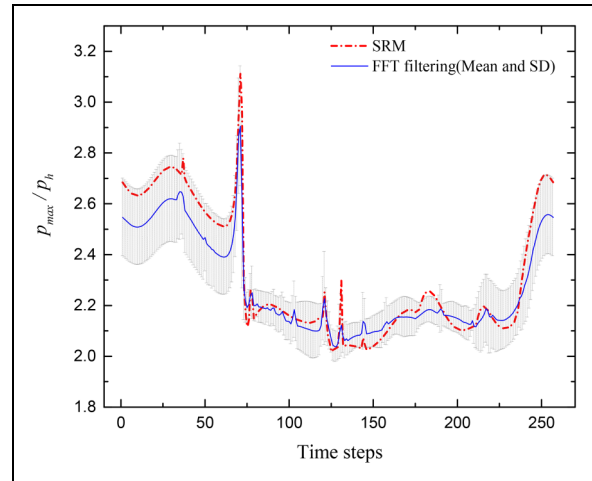


Figure 7. Mean gap u_g values with fractal surfaces simulated by FFT filtering and SRM. FFT: fast Fourier transform; SRM: spectral representation method.

Table 2. Parameters for the elastohydrodynamic lubrication (EHL) simulation.

Parameter	Value
Ball radius, R_x/m	1.27×10^{-2}
Maximum Hertzian contact pressure, p_H/Pa	0.54×10^9
Equivalent Young's modulus, E^*/Pa	1.17×10^{11}
Ambient viscosity, $\eta_0/\text{Pa}\cdot\text{s}$	1.22
Non-dimensional velocity, $U = \eta_0 u_s / (2E^* R_x)$	4×10^{-11}
Pressure-viscosity coefficient, α/Pa^{-1}	2.25×10^{-8}
Hertzian contact radius, b/m	1.84×10^{-4}

amount as the transient EHL is considered. All the simulated surfaces were sampled down to the size of 256×256 to save computational resources further. One thing to note is that the sampling-down process is not a recommended method to generate rough surfaces for EHL simulation, and it is used here only for numerical convenience. If one wants to run some accurate EHL simulations, it is better to regenerate rough surfaces after adjusting the mesh size and cutoff frequencies. The time step was set to the value, making the surface move one mesh grid at each time step. Such a setting means that after every 257 time steps, the roughness matrix is cycled once. The total number of time steps was set to 13 times the time steps needed for one cycle of the surface, by which the transient system reaches a steady state. The root-mean-square roughness value was reduced to $0.0762 \mu\text{m}$ to avoid any asperity contacts in the Hertzian contact zone. It should also be noted that the solution domain is a square area whose side length is four times the radius of the Hertzian contact zone, which is bigger than the area of the simulated surfaces ($0.1 \text{ mm} \times 0.1 \text{ mm}$). Here to simplify the simulation setup, all the simulated surfaces were assigned to the mesh of the solution domain. The simulations ran on the ARC3, part of the high-performance computing facilities at the University of Leeds, UK, with E5-2650v4 CPU, 2.2 GHz.

**Figure 8.** Minimum film thickness, h_{min} values of the last cycle of surface.**Figure 9.** Maximum pressure, p_{max} values of the last cycle of surface.

Based on the simulation results, the minimum film thickness h_{min} and maximum pressure p_{max} were extracted. The h_{min} and p_{max} values from the last 257 time steps were plotted in Figures 8 and 9, respectively. Figure 8 shows that the h_{min} resulting from the SRM-generated surface has a similar trend with the mean h_{min} calculated using the FFT filtering method simulated surfaces, but the specific values vary significantly. The curves in Figure 9 show the p_{max} results in the same manner. The mean p_{max} values calculated using the FFT filtering method simulated surfaces have almost the same trend as the p_{max} values obtained using the surface generated by the SRM. Generally, the parameters of interest calculated in the transient problem are averaged in the last complete surface cycle to represent the steady-state results. Therefore, the h_{min} and p_{max} values in the last cycle were averaged. With the surface simulated by the SRM, the averaged h_{min} and p_{max} are $0.282 \mu\text{m}$ and $2.32p_H\text{Pa}$, respectively. For the surfaces simulated by the FFT filtering method, the averaged h_{min} and p_{max} are $0.284 \mu\text{m}$ and $2.28p_H\text{Pa}$, respectively. From this perspective, the results obtained with surfaces simulated by the FFT filtering method and SRM match each other. However, compared with the results of rough surface contact, using the FFT filtering method or SRM has a more significant influence on EHL performance prediction. It is worth mentioning that each transient EHL simulation here needs around 25 h to finish. Using 10 rough surfaces generated by the FFT filtering method means around 250 h. This considerable cost can be reduced just by using the one rough surface simulated by the SRM.

In summary, the FFT filtering method introduces one more source of uncertainties, the amplitude term in equation (2), in the simulated surfaces compared with the SRM. When the phase term, the common source of uncertainties in the two methods, is fixed, the FFT filtering method generates surfaces whose mean profile approaches the unique surface generated by the SRM. Moreover, the FFT filtering method introduces uncertainties in the PSD of simulated surfaces, while the SRM can

perfectly reproduce the given power-law PSD. Furthermore, through a preliminary analysis of roughness parameters, the two sources of uncertainties (amplitude and phase) in the FFT filtering method are probably irrelevant. Testing the two methods with the rough contact and EHL simulations demonstrates that one SRM simulated surface can represent the averaged results from several surfaces simulated by the FFT filtering method when the phase term is fixed. Hence, the SRM seems to be a better method to generate accurate and representative fractal rough surfaces for predicting tribological performance. However, this does not mean that using the FFT filtering method is wrong, as real measured surfaces have uncertainties in their PSDs. Considering such uncertainties or not needs comprehensive studies about their influences on tribological properties in different applications. Based on the analysis in this paper, the uncertainties in PSD do not affect scenarios where the average influence of rough surfaces is more important. Such results do not rule out that some applications in which the extreme conditions matter and the uncertainties in PSD have a significant impact, for example, fluid sealing and micropitting. Therefore, we recommend the SRM when the average influence of rough surfaces is of more concern.

The influence of low and high cutoff frequencies

To better understand the effect of cutoff frequency on the normality of simulated fractal surfaces, the PSD with and without roll-off is investigated with different low and high cutoff frequencies in this section. Moreover, the traditional non-fractal exponential PSD is used as a comparison. Based on the discussions in the section Surfaces generated by the FFT filtering method and SRM, only the SRM is used here for numerical efficiency.

According to previous work considering the cutoff frequencies in simulating fractal surfaces,^{12,37,38} the ratios of

low (high) cutoff frequency to the lower bound (upper bound) of the frequency range of the surface are essential parameters affecting the normality of simulated surfaces. In the current work, the ratio of low cutoff frequency, q_l , to the lower bound of the surface frequency range, q_{min} , was set as $q_l/q_{min} = 1, 1.4, 2.5, 5$, and 10 . The ratio of high cutoff frequency, q_s , to the upper bound of the surface frequency range, q_{max} , was set as $q_s/q_{max} = 0.1, 0.14, 0.24, 0.5$, and 1 . While altering the q_l/q_{min} values, the q_s/q_{max} was fixed at 1 . When the different q_s/q_{max} values were used, the q_l/q_{min} was set at one. Furthermore, for roll-off PSD, the roll-off wavelength in equation (5), λ_r was fixed at $20 \mu\text{m}$, while for single power-law PSD, λ_r equaled $100 \mu\text{m}$ to remove the plateau region in PSD shown in equation (5).

For each different cutoff frequency value, 1000 surfaces were generated with different ϕ_{kl} values. Furthermore, all the simulated surfaces were normalized to zero mean and unit standard deviation. To quantitatively evaluate the normality of the simulated surfaces, the histogram of the simulated surface was calculated and compared with the standard Gaussian distribution histogram. Furthermore, the differences between the histogram of simulated surfaces and the standard Gaussian distribution were calculated as errors referring to Pérez-Ràfols and Almqvist.³⁶ The histogram of a set of random data is calculated by dividing the range of the data set into intervals covering the lowest to the highest value of the data set. Such intervals are referred to as bins. The frequency, n_i is the number of heights falling in the specific interval over the total number of data points. The number of bins is chosen based on Scott's rule, which is automatically implemented by MATLAB. The histograms of simulated surfaces and standard Gaussian distribution used the same bins. Therefore, the error of histogram, e_h is calculated

$$e_h = \sum_{i=1}^{N_b} |n_{is} - n_{it}| w_b \quad (9)$$

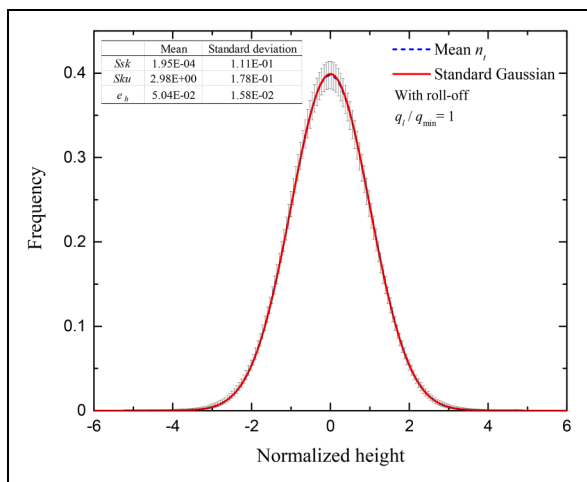


Figure 10. Mean histogram of simulated surfaces and corresponding standard deviation with roll-off power spectral density (PSD), $q_l/q_{min} = 1$.

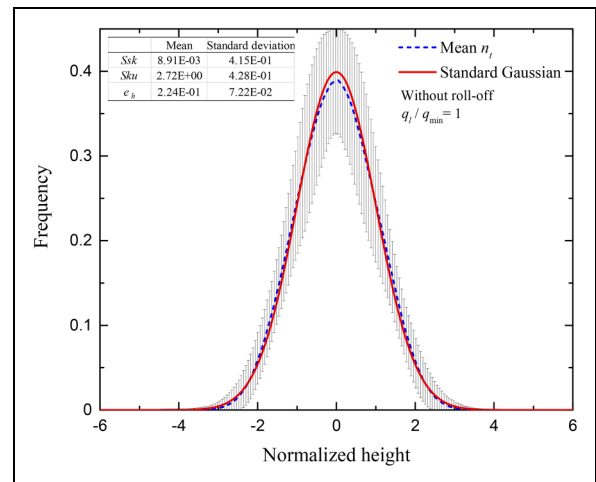


Figure 11. Mean histogram of simulated surfaces and corresponding standard deviation with single power-law power spectral density (PSD), $q_l/q_{min} = 1$.

where n_{is} is the frequency of histogram of simulated surfaces, n_{it} is the frequency of standard Gaussian distribution, w_b is the width of bins, and N_b is the number of bins.

First of all, the influence of low cutoff frequency is analyzed. Figure 10 shows the mean histogram of simulated surfaces with roll-off PSD and the corresponding standard deviation for $q_l/q_{min} = 1$. The standard Gaussian histogram was also plotted as a reference. The mean histogram of simulated surfaces matches well with the standard Gaussian, showing good normality. However, the corresponding SD shows that each simulated surface histogram could significantly deviate standard Gaussian, especially near the surface mean height. The mean e_h of simulated surface histograms is 5.04×10^{-2} , quantifying the degree of such deviation. In Figure 11, the histograms of simulated surfaces with single power-law PSD were plotted for $q_l/q_{min} = 1$. The results clearly show that even the mean histogram of simulated surfaces has significant discrepancies with the standard Gaussian. The corresponding standard deviation values are much larger than those shown in Figure 10, resulting in a larger mean $e_h = 2.24 \times 10^{-1}$. Figure 12 shows the histogram when $q_l/q_{min} = 10$, by which the q_l is greater than the roll-off frequency q_r , means that the PSD with or without roll-off gives the same pattern. Thus, the histograms shown in Figure 12 represent the results for $q_l/q_{min} = 10$ whether the PSD with roll-off or not. In Figure 12, it is readily seen that the mean histogram of simulated surfaces has a better agreement with the standard Gaussian, and the corresponding SD values are smaller than those in Figures 10 and 11, providing a mean e_h as small as 1.85×10^{-2} .

Furthermore, Figure 13 shows the mean e_h values and corresponding SD values with different q_l/q_{min} values. As the q_l/q_{min} increases, the mean e_h decreases, and the corresponding SD also decreases. Also, roll-off PSD dramatically reduces the mean e_h values and SDs when the q_l/q_{min} value is close to 1. These results mean that, first, a large q_l/q_{min} value, for example, >5 , can sufficiently improve the normality of each simulated surface, as the

mean e_h values and their SDs are reduced simultaneously. Second, with the PSD showing a plateau region, meaning roll-off frequency is larger than the low cutoff frequency, the q_l/q_{min} value has a much weaker effect on the normality of the simulated surfaces. Therefore, if inevitable, for PSD with a plateau region, q_l/q_{min} value could equal 1 to generate Gaussian fractal surfaces having acceptable normality. However, for the single power-law PSD, the q_l/q_{min} value shall be at least >1 , which is also suggested by Yastrebov et al.¹²

Next, the different q_s/q_{max} values were used to simulate surfaces. Figure 14 shows the mean e_h values and corresponding SD values with various q_s/q_{max} values for PSD with and without the plateau region. The results prove that the q_s/q_{max} does not affect the normality of simulated surfaces whether the PSD has a plateau region or not.

In comparison, the exponential PSD for the simulation of non-fractal surfaces was tested. The exponential PSD was calculated by the Fourier transform of the exponential ACF, which is defined by $R(p, q) = \exp[\log(0.1)\sqrt{(p/30)^2 + (q/30)^2}]$. The q_l/q_{min} and q_s/q_{max} both equal 1. Figure 15 plots the mean histogram and corresponding SD of simulated surfaces with exponential PSD. It clearly shows that the mean histogram of simulated surfaces matches the standard Gaussian with a tiny SD. Comparing Figure 15 with Figure 12, the magnitude of the SD in Figure 15 is much smaller than that in Figure 12. Such phenomenon is reflected by the e_h value as well. For Figure 15, the mean e_h value is 9.61×10^{-3} , which is smaller than 1.85×10^{-2} in Figure 12. It is worth mentioning that the q_l/q_{min} value equals 1 for the results in Figure 15 but equals 10 for those in Figure 12. These results mean one can ignore the influence of q_l/q_{min} when the target PSD is exponential. Therefore, it seems that the significant influence of q_l/q_{min} on the normality of simulated surfaces is a particular case resulted from the power-law PSD and only needs to be considered for the simulation of fractal surfaces.

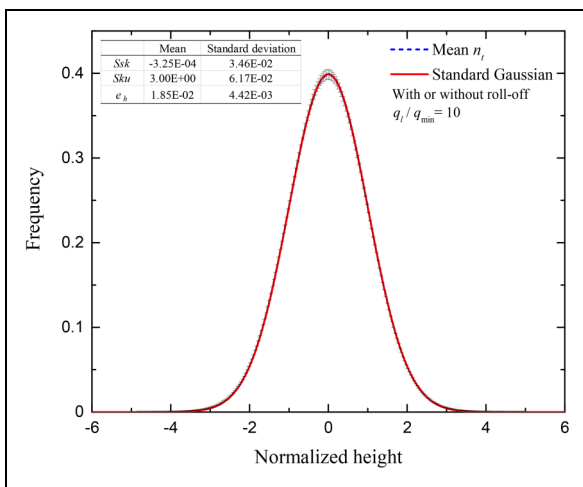


Figure 12. Mean histogram of simulated surfaces and corresponding standard deviation with or without power spectral density (PSD) roll-off, $q_l/q_{min} = 10$.

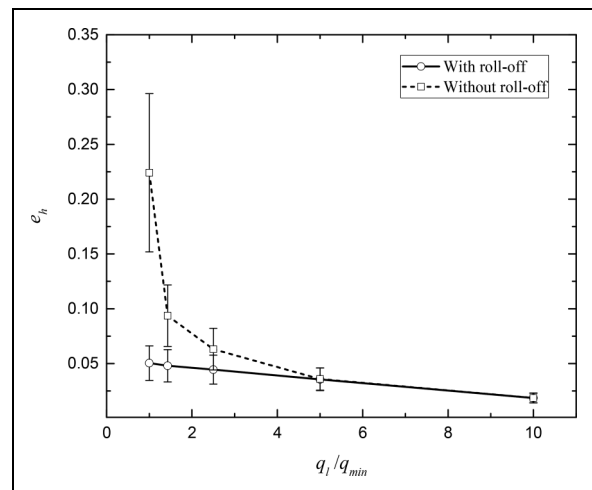


Figure 13. Mean histogram error e_h and corresponding standard deviation for different q_l/q_{min} values.

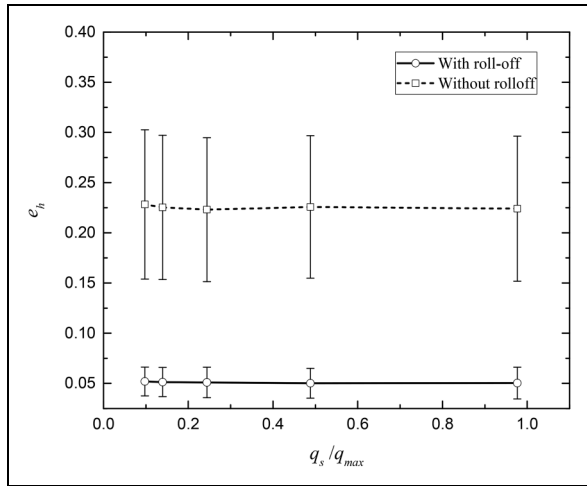


Figure 14. Mean histogram error e_h and corresponding standard deviation for different q_s/q_{max} values.

Simulation of non-Gaussian fractal surfaces

The method of Wang et al.²⁴ was tested to simulate a fractal surface indexed as NG-1 with $Ssk = -1$ and $Sku = 7$. Considering the brevity of this paper, we do not include the validation of the method implementation here. Relevant details will be provided according to the requirements of readers. The PSD of the simulated surface was plotted in Figure 16 together with the target PSD. The results show that huge discrepancies exist between the simulated and target PSDs. This phenomenon is very different from the high accuracy reported by Wang et al.²⁴ It is not difficult to infer that the reason behind such different behavior is about altering the exponential PSD to power-law PSD. The procedures used to find the underlying PSD (see section Simulation of non-Gaussian rough surfaces and Wang et al.²⁴) do not work well with the power-law PSD, and the quality of the underlying PSD corresponding to the power-law PSD is poor. Therefore,

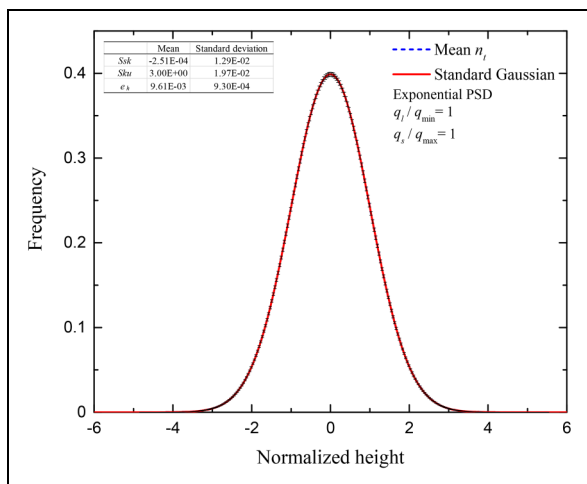


Figure 15. Mean histogram of simulated surfaces and corresponding standard deviation with exponential power spectral density (PSD), $q_l/q_{min} = 1$, $q_s/q_{max} = 1$.

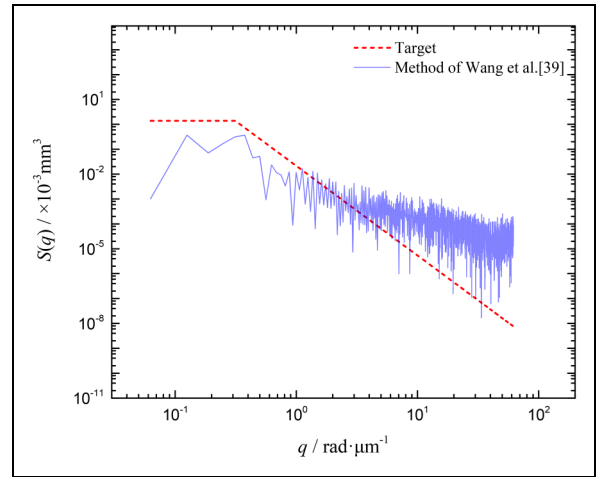


Figure 16. Target power spectral density (PSD) and PSD of one NG-1 fractal surface simulated by the method of Wang et al.²⁴

the Wang et al.²⁴ method is not the proper choice to generate non-Gaussian fractal surfaces.

Based on the attempt to simulate the non-Gaussian fractal rough surfaces above, it can be inferred that the power-law PSD limits the ability of SRM in generating non-Gaussian surfaces. Therefore, a compromise between reproducing the power-law PSD and non-Gaussian height distribution should be made to simulate non-Gaussian fractal surfaces. In that case, what if directly translating simulated Gaussian surfaces to non-Gaussian surfaces by the Johnson translator system?

In the current work, this idea was tested. Firstly, Gaussian fractal rough surfaces were simulated by the SRM. Then, the Gaussian surfaces were translated to non-Gaussian surfaces with the parameters listed in Table 3 by the Johnson translator system. These parameters are chosen to cover the range of Ssk and Sku values of surfaces machined by the most common machining processes.⁴⁶ As the generated Gaussian surfaces are not

Table 3. Ssk and Sku values of the simulated non-Gaussian surfaces.

Surface index	Ssk			Sku		
	Target	Simulated	Error/%	Target	Simulated	Error/%
NG-1	-1	-1.037	3.72	7	6.759	3.45
NG-2	-1	-1.033	3.34	14	14.60	4.31
NG-3	-1	-1.085	8.54	25	26.90	7.61
NG-4	1	1.006	0.65	7	6.837	2.32
NG-5	1	1.040	4.01	14	14.12	0.89
NG-6	1.6	1.562	2.40	7	6.902	1.40
NG-7	-1.6	-1.555	2.80	7	6.870	1.85
NG-8	-3	-2.956	1.44	14	13.43	4.06
NG-9	-3	-3.066	2.18	25	24.05	3.80
NG-10	3	3.062	2.08	25	25.92	3.66
NG-11	-4	-4.104	2.59	50	46.86	6.28
NG-12	4	3.915	2.13	50	45.86	8.29

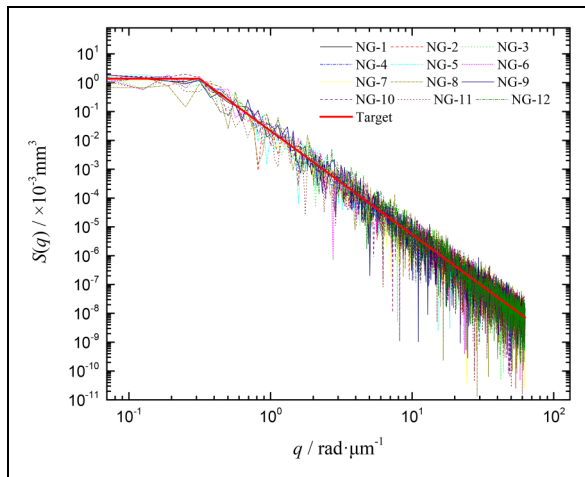


Figure 17. Power spectral density (PSD) values of the simulated non-Gaussian fractal surfaces.

ideal, some translated surfaces could have significant errors in reproducing S_{sk} and S_{ku} values, and these surfaces should be discarded and regenerated. It is worth mentioning that Francisco and Brunetiere⁴² provided a hybrid method to improve the accuracy of translated non-Gaussian series. Therefore, if one needs high accuracy non-Gaussian surfaces, the hybrid method is worth trying.

Figure 17 shows the PSDs of surfaces generated by the different parameters in Table 3. It clearly shows that all the PSD curves follow the target power-law PSD approximately. Moreover, although the translation process causes variations in the PSD values, it still gives better agreement with the target power-law PSD than the method of Wang et al.²⁴ (Figure 16). The next task is evaluating the reproduction of the target S_{sk} and S_{ku} values. The corresponding values of each simulated surface and the relative errors are listed in Table 3 as well. It can be seen that most of the simulated surfaces have relative errors of <5%, and the highest relative error is still <10%, which means a sound reproduction of the target S_{sk} and S_{ku} values.

Therefore, by directly translating simulated Gaussian surfaces to non-Gaussian surfaces through the Johnson translator system, a compromise between the accuracy of the PSD and the non-Gaussian height distribution is achieved. This method provides a straightforward way to simulate non-Gaussian fractal surfaces, as no iterative steps are included. One should keep in mind that this method is approximate and can be used when the uncertainties in the PSD do not affect the specific applications much. If high accuracy of the PSD and height distribution is required, some more complex methods should be considered, such as the work of Pérez-Ráfols and Almqvist³⁶ and Francisco and Brunetiere.⁴²

Conclusions

This paper studied the application of the spectral representation method (SRM) in generating Gaussian and non-Gaussian fractal rough surfaces and compared it

with the traditional FFT filtering method. The influences of PSD cutoff frequencies were also investigated. The main conclusions are as follows:

1. The FFT filtering method has two sources of uncertainties theoretically, PSD as the amplitude term and the phase term, which are probably irrelevant according to the preliminary analysis of roughness parameters in this paper.
2. Compared with the FFT filtering method, the SRM does not introduce uncertainties in the PSD, which gives the SRM advantages in predicting statistical quantities in tribology analysis. One single rough surface generated by the SRM can instead take average results obtained using dozens of surfaces generated by the FFT filtering method, reducing the cost of computation resources significantly. For some applications where the extreme conditions, not averaged results, are important, the FFT filtering method might still be needed to include uncertainties in the PSD.
3. The ratio of high cutoff frequency, q_s , to the upper bound of the frequency range, q_{max} , does not significantly affect the normality of simulated Gaussian fractal surfaces.
4. The ratio of low cutoff frequency, q_l , to the lower bound of the frequency range, q_{min} , significantly influences the normality of simulated Gaussian fractal surfaces. Increasing the q_l/q_{min} value can improve the normality of the simulated Gaussian fractal surfaces. Such improvement for the PSD without roll-off is more significant than that for the roll-off PSD. For the PSD without roll-off, the q_l/q_{min} value shall be at least >1.
5. Compared with using the power-law PSD, the q_l/q_{min} has nearly zero effect on the normality of simulated Gaussian surfaces using an exponential PSD, which indicates such influence might be a particular case along with the power-law PSD.
6. Directly translating Gaussian fractal surfaces simulated by the SRM to non-Gaussian surfaces through the Johnson translator system compromises the accuracy of the PSD to reproduce non-Gaussian properties. It could be used as an approximate but fast method to generate non-Gaussian fractal surfaces when the uncertainties in the PSD do not significantly affect the specific applications.

Acknowledgements

This work was undertaken on ARC3, part of the High-Performance Computing facilities at the University of Leeds, UK.


Declaration of Conflicting Interests


The author(s) declared no potential conflicts of interest with respect to the research, authorship, and/or publication of this article.

Funding

The author(s) disclosed receipt of the following financial support for the research, authorship, and/or publication of this article: This work was supported by the Engineering and Physical Sciences Research Council (grant number EP/001766/1”) as a part of ‘Friction: The Tribology Enigma’ Programme Grant (www.friction.org.uk), and TRibology as an ENabling Technology (TRENT) EP/S030476/1). Supplemental material for this article is available online.

ORCID iDs

Yuechang Wang  <https://orcid.org/0000-0002-0830-4434>

Arđian Morina  <https://orcid.org/0000-0001-8868-2664>

References

- Persson BNJ. On the fractal dimension of rough surfaces. *Tribol Lett* 2014; 54: 99–106.
- Sayles RS and Thomas TR. Surface topography as a nonstationary random process. *Nature* 1978; 271: 431–434.
- Majumdar A and Bhushan B. Role of fractal geometry in roughness characterization and contact mechanics of surfaces. *J Tribol* 1990; 112: 205–216.
- Majumdar A and Tien CL. Fractal characterization and simulation of rough surfaces. *Wear* 1990; 136: 313–327.
- Ganti S and Bhushan B. Generalized fractal analysis and its applications to engineering surfaces. *Wear* 1995; 180: 17–34.
- Peklenik J. Paper 24: new developments in surface characterization and measurements by means of random process analysis. *Proc Inst Mech Eng, Conf Proc* 1967; 182: 108–126.
- Nayak PR. Random process model of rough surfaces. *J Lubr Technol* 1971; 93: 398–39&.
- Persson BNJ, Albohr O, Tartaglino U, et al. On the nature of surface roughness with application to contact mechanics, sealing, rubber friction and adhesion. *J Phys: Condens Matter* 2004; 17: R1–R62.
- Müser MH, Dapp WB, Bugnicourt R, et al. Meeting the Contact-Mechanics Challenge. *Tribol Lett* 2017; 65, 118 (2017).
- Majumdar A and Bhushan B. Fractal model of elastic-plastic contact between rough surfaces. *J Tribol* 1991; 113: 1–11.
- Dapp WB, Lucke A, Persson BN, et al. Self-affine elastic contacts: percolation and leakage. *Phys Rev Lett* 2012; 108: 244301.
- Yastrebov VA, Anciaux G and Molinari J-F. From infinitesimal to full contact between rough surfaces: evolution of the contact area. *Int J Solids Struct* 2015; 52: 83–102.
- Papangelo A, Hoffmann N and Ciavarella M. Load-separation curves for the contact of self-affine rough surfaces. *Sci Rep* 2017; 7: 6900.
- Li L and Yang J. Surface roughness effects on point contact elasto-hydrodynamic lubrication in linear rolling guide with fractal surface topographies. *Ind Lubr Tribol* 2018; 70: 589–598.
- Zhang X, Xu Y and Jackson RL. A mixed lubrication analysis of a thrust bearing with fractal rough surfaces. *Proc Inst Mech Eng, Part J: J Eng Tribol* 2019; 234: 608–621.
- Pawlus P, Reizer R and Wieczorowski M. A review of methods of random surface topography modeling. *Tribol Int* 2020; 152: 106530.
- Patir N. Numerical procedure for random generation of rough surfaces. *Wear* 1978; 47: 263–277.
- Hu YZ and Tonder K. Simulation of 3-d random rough-surface by 2-d digital-filter and Fourier-analysis. *Int J Mach Tools Manuf* 1992; 32: 83–90.
- Bakolas V. Numerical generation of arbitrarily oriented non-Gaussian three-dimensional rough surfaces. *Wear* 2003; 254: 546–554.
- Minet C, Brunetiere N, Tourmerie B, et al. Analysis and modeling of the topography of mechanical seal faces. *Tribol Trans* 2010; 53: 799–815.
- Newland DE. *An introduction to random vibration and spectral analysis*. 2nd ed. London: Longman, 1984.
- Wu JJ. Simulation of rough surfaces with FFT. *Tribol Int* 2000; 33: 47–58.
- Wu J-J. Simulation of non-Gaussian surfaces with FFT. *Tribol Int* 2004; 37: 339–346.
- Wang Y, Liu Y, Zhang G, Wang Y, et al. (October 4, 2017). A Simulation Method for Non-Gaussian Rough Surfaces Using Fast Fourier Transform and Translation Process Theory. *ASME. J. Tribol. March* 2018; 140(2): 021403.
- Johnson NL. Systems of frequency curves generated by methods of translation. *Biometrika* 1949; 36: 149–176.
- Voss RF. *Random fractal forgeries*. Berlin, Heidelberg: Springer Berlin Heidelberg, 1985, pp.805–835.
- Voss RF. Fractals in nature: from characterization to simulation. In: Peitgen H-O and Saupe D (eds) *The science of fractal images*. New York, NY: Springer New York, 1988, pp.21–70.
- Saupe D. Algorithms for random fractals. In: Peitgen H-O and Saupe D (eds) *The science of fractal images*. New York, NY: Springer New York, 1988, pp.71–136.
- Wu JJ. Characterization of fractal surfaces. *Wear* 2000; 239: 36–47.
- Borri C and Paggi M. Topology simulation and contact mechanics of bifractal rough surfaces*. *Proc Inst Mech Eng Part J-J Eng Tribol* 2016; 230: 1345–1358.
- Pei L, Hyun S, Molinari JF, et al. Finite element modeling of elasto-plastic contact between rough surfaces. *J Mech Phys Solids* 2005; 53: 2385–2409.
- Bonari J, Marulli MR, Hagemeyer N, et al. A multiscale FEM-BEM formulation for contact mechanics between rough surfaces. *Comput Mech* 2020; 65: 731–749.
- Paggi M and Ciavarella M The coefficient of proportionality κ between real contact area and load, with new asperity models. *Wear* 2010; 268: 1020–9.
- Putignano C, Afferrante L, Carbone G, et al. A new efficient numerical method for contact mechanics of rough surfaces. *Int J Solids Struct* 2012; 49: 338–343.
- Zou M, Yu B, Feng Y, et al. A Monte Carlo method for simulating fractal surfaces. *Physica A* 2007; 386: 176–186.
- Pérez-Ráfols F and Almqvist A. Generating randomly rough surfaces with given height probability distribution and power spectrum. *Tribol Int* 2019; 131: 591–604.
- Pérez-Ráfols F and Almqvist A. On the stiffness of surfaces with non-Gaussian height distribution. *Sci Rep* 2021; 11: 1863.

38. Prodanov N, Dapp WB and Müser MH. On the contact area and mean gap of rough, elastic contacts: dimensional analysis, numerical corrections, and reference data. *Tribol Lett* 2014; 53: 433–448.
39. Shinozuka M and Deodatis G. Simulation of stochastic processes by spectral representation. *Appl Mech Rev* 1991; 44: 191–204.
40. Watson W and Spedding TA. The time-series modeling of non-Gaussian engineering processes. *Wear* 1982; 83: 215–231.
41. Hill ID, Hill R and Holder RL. Fitting Johnson curves by moments. *Appl Stat* 1976; 25: 180–184.
42. Francisco A and Brunetiere N. A hybrid method for fast and efficient rough surface generation. *Proc Inst Mech Eng, Part J: J Eng Tribol* 2015; 230: 747–768.
43. Lou S, Pagani L, Zeng W, et al. Watershed segmentation of topographical features on freeform surfaces and its application to additively manufactured surfaces. *Prec Eng* 2020; 63: 177–186.
44. Marklund P, Lugt PM, Almqvist A, et al. A mixed lubrication model incorporating measured surface topography. Part 1: theory of flow factors. *Proc Inst Mech Eng, Part J: J Eng Tribol* 2010; 224: 335–351.
45. Venner CH and Lubrecht AA. Numerical analysis of the influence of waviness on the film thickness of a circular EHL contact. *J Tribol* 1996; 118: 153.
46. Whitehouse DJ. *Handbook of surface and nanometrology*. 2nd ed, Boca Raton, CRC Press, 2010.

Appendix

Notation

a_r	relative contact area
b	Hertzian contact radius
e_h	the error of histogram of simulated surfaces
h_{min}	minimum film thickness
n_{is}	the frequency of histogram of simulated surfaces
n_{it}	the frequency of standard Gaussian distribution
p_c	mean contact pressure
p_h	maximum Hertzian contact pressure
p_{max}	maximum pressure
q	angular frequency
q_r	roll-off angular frequency
q_l	low cutoff frequency
q_s	high cutoff frequency
q_{min}	lowest cutoff frequency determined by the surface dimensions
q_{max}	highest cutoff frequency determined by the surface dimensions
u_g	mean gap
w_b	the width of bins
x	Gaussian series
z_{ij}	surface height at the point (i, j)
B_{kl}	parameter related to the PSD value at the point (k, l)
D	fractal dimension
E^*	equivalent Young's modulus
H	Hurst roughness exponent

L	linear dimension in x and y directions of the target surface
M, N	size of surface mesh
N_b	the number of bins
S_{kl}	PSD value at the point (k, l)
Ssk	skewness of a random series
Sku	kurtosis of a random series
Sds	summit density
Sdq	root-mean-square gradient of rough surface
Rc	mean summit radius
R_x	ball radius
U	non-dimensional velocity
α	pressure-viscosity coefficient
α_{kl}	random number uniformly distributed between $[0, 1]$
σ^2	variance of a random series
η	non-Gaussian series
η_0	ambient viscosity
$\nu, \delta, \xi, \lambda$	parameters in the Johnson translator system
λ_r	roll-off wavelength
λ_s	short-wavelength cutoff
μ	mean value of a random series
ϕ_{kl}	random phase at the point (k, l)

Appendix A

The equation to generate random surfaces is the following,

$$z_{ij} = \sum_{k=0}^{M-1} \sum_{l=0}^{N-1} B_{kl} \exp(i\phi_{kl}) \exp\left[i\left(\frac{2\pi ki}{M} + \frac{2\pi lj}{N}\right)\right] \quad (A1)$$

No matter the FFT filtering or the SRM are used, B_{kl} satisfies the following equation.

$$B_{kl} \propto S_{kl} \quad (A2)$$

It should be noted that B_{00} must always be zero. With the usage of FFT, the following equations are met by default,

$$\begin{aligned} M\Delta x &= L_x = \frac{2\pi}{\Delta\omega_x} \\ N\Delta y &= L_y = \frac{2\pi}{\Delta\omega_y} \end{aligned} \quad (A3)$$

$$\begin{aligned} \Delta\omega_x &= \frac{\omega_{xu}}{m} \\ \Delta\omega_y &= \frac{\omega_{yu}}{n} \end{aligned} \quad (A4)$$

where Δx and Δy are the spacing lengths, L_x and L_y are the side lengths, $\Delta\omega_x$ and $\Delta\omega_y$ are the angular frequencies, M and N are the discrete points for the surface, m and n are the discrete points for the PSD, ω_{xu} and ω_{yu} are the high cutoff frequencies, in x and y directions, respectively.

To avoid aliasing, the spacing lengths have to obey the condition:

$$\begin{aligned}\Delta x &\leq \frac{2\pi}{2\omega_{xu}} \\ \Delta y &\leq \frac{2\pi}{2\omega_{yu}}\end{aligned}\quad (A5)$$

Combining equations (A5), (A4), and (A3), the following conditions are established:

$$\begin{aligned}M &\geq 2m \\ N &\geq 2n\end{aligned}\quad (A6)$$

Usually, the equal sign in equation (A6) is taken in the numerical procedures.

Based on equation (A6), it is evident that only a quarter of the full B_{kl} can be calculated from the PSD. The full B_{kl} can be obtained symmetrically by

$$\begin{aligned}B_{M-k,N-l} &= B_{k,N-l} = B_{M-k,l} = B_{k,l} \\ k &= 0, 1, 2, \dots, m \\ l &= 0, 1, 2, \dots, n\end{aligned}\quad (A7)$$

To avoid the imaginary part after inverse FFT is conducted, the ϕ_{kl} should obey the following equations:

$$\begin{aligned}\phi_{k,l} &= -\phi_{M-k,N-l} \\ \phi_{k,0} &= -\phi_{M-k,0} \\ \phi_{0,l} &= -\phi_{0,N-l} \\ \phi_{0,0} &= \phi_{0,n} = \phi_{m,0} = \phi_{m,n} = 0 \\ k &= 0, 1, 2, \dots, m \\ l &= 0, 1, 2, \dots, n\end{aligned}\quad (A8)$$

Appendix B

Skewness, Ssk :

$$Ssk = \frac{1}{\sigma^3} \frac{\sum_{i=1}^M \sum_{j=1}^N z_{ij}^3}{MN}\quad (B1)$$

Kurtosis, Sku :

$$Sku = \frac{1}{\sigma^4} \frac{\sum_{i=1}^M \sum_{j=1}^N z_{ij}^4}{MN}\quad (B2)$$

For an ideal Gaussian distribution, the Ssk equals 0, and the Sku equals 3.

Root-mean-square gradient, Sdq :

$$Sdq = \sqrt{\frac{1}{A} \iint_A \left[\left(\frac{\partial z(x,y)}{\partial x} \right)^2 + \left(\frac{\partial z(x,y)}{\partial y} \right)^2 \right] dx dy}\quad (B3)$$

where A is the area of the simulated surface.

The density of summits, Sds :

$$Sds = \frac{n_s}{A}\quad (B4)$$

where n_s is the number of summits identified by the eight nearest neighbor method.

The Rc is the average curvature radius of each summit. For a summit whose position is indexed as (i, j) , the corresponding curvature radius is

$$radius(i, j) = - \left[\frac{1}{2} \left(\frac{\partial^2 z(x_i, y_j)}{\partial x_i^2} + \frac{\partial^2 z(x_i, y_j)}{\partial y_j^2} \right) \right]^{-1}\quad (B5)$$

Then, the Rc can be calculated by

$$Rc = \frac{1}{n_s} \sum_1^{n_s} radius(i, j)\quad (B6)$$